GEOLOGICA CARPATHICA, APRIL 2016, 67, 2, 121–132 doi: 10.1515/geoca-2016-0008

The Schwarzhorn Amphibolite (Eastern Rätikon, Austria): an Early Cambrian intrusion in the Lower Austroalpine basement

NILS-PETER NILIUS[1,2], NIKOLAUS FROITZHEIM[1], THORSTEN JOACHIM NAGEL[3], FRANK TOMASCHEK[1] and ALEXANDER HEUSER[1]

[1]Steinmann-Institut, Universität Bonn, Poppelsdorfer Schloss, D-53115 Bonn, Germany; nilius@geowi.uni-hannover.de
[2] Present adress: Institut für Geologie, Leibniz Universität Hannover, Callinstraße 30, D-30167 Hannover, Germany
[3] Department of Geoscience, Aarhus University, Høegh-Guldbergs Gade 2, 8000 Aarhus C, Denmark

(Manuscript received May 8, 2015; accepted in revised form December 8, 2015)

Abstract: The Alpine nappe stack in the Penninic-Austroalpine boundary zone in the Rätikon (Austria) contains a 4×1 km tectonic sliver of meta-diorite, known as the Schwarzhorn Amphibolite. It was deformed and metamorphosed in the amphibolite facies and is unconformably overlain by unmetamorphic Lower Triassic sandstone, indicating pre-Triassic metamorphism. Cataclastic deformation and brecciation of the amphibolite is related to normal faulting and block tilting during Jurassic rifting. Zircon dating of the Schwarzhorn Amphibolite using LA-ICP-MS gave a U-Pb age of 529+9/–8 Ma, interpreted as the crystallization age of the protolith. Geochemical characteristics indicate formation of the magmatic protolith in a supra-subduction zone setting. The Cambrian protolith age identifies the Schwarzhorn Amphibolite as a pre-Variscan element within the Austroalpine basement. Similar calc-alkaline igneous rocks of Late Neoproterozoic to Early Cambrian age are found in the Upper Austroalpine Silvretta Nappe nearby and in several other Variscan basement units of the Alps, interpreted to have formed in a peri-Gondwanan active-margin or island-arc setting.

Keywords: Rätikon, Lower Austroalpine, Arosa Zone, pre-Alpine basement, Jurassic rifting, U-Pb zircon geochronology.

Introduction

The present study concerns the Schwarzhorn Amphibolite, a sliver of meta-diorite exposed in the Penninic-Austroalpine boundary zone in the Tilisuna area, NE Rätikon (Fig. 1). Field relations suggested a pre-Mesozoic age for the metamorphic overprint and in consequence also for the protolith (Nagel 2006). It was therefore interpreted as part of the Variscan basement of the Lower Austroalpine nappes. So far, the reported protolith ages in Lower Austroalpine basement units are Carboniferous and Permian (Spillmann & Büchi 1993; von Quadt et al. 1994). Here, we determine the protolith age of the Schwarzhorn Amphibolite and the tectonic setting in which its magmatic precursor was emplaced.

Geological outline

A stack of Lower Penninic to Upper Austroalpine nappes is exposed along the Penninic-Austroalpine boundary in eastern Graubünden (Switzerland) and adjacent Vorarlberg (Austria). The structurally deepest position is occupied by Lower Penninic Bündnerschiefer and flysch units, the highest by Upper Austroalpine crystalline basement with its locally preserved Mesozoic sedimentary cover. The trace of this boundary is characterized by an eastward embayment of the Penninic into the Austroalpine; the Prättigau half-window (Fig. 1 inset). Imbricated along the Penninic-Austroalpine boundary, thin nappes and slices of Middle Penninic, Upper Penninic and Lower Austroalpine origin are exposed.

South of the Prättigau half-window, Upper Penninic and Lower Austroalpine nappes exhibit remnant Jurassic-age structures of the non-volcanic passive continental margin of the Adriatic continent. Kinematics and architecture of Early to Middle Jurassic rifting and the subsequent opening of the Piemont-Ligurian Ocean have been extensively studied in the last decades (Eberli 1988; Froitzheim & Eberli 1990; Froitzheim & Manatschal 1996; Handy 1996; Mohn et al. 2010, 2011). Penninic and Austroalpine nappes in SE Graubünden were assigned to their former positions on the margin. The Platta and Malenco Nappes display the ocean-continent transition. The Err Nappe represents a distal remnant of the Adriatic passive margin, characterized by westward (oceanward) dipping normal faults, whereas the Bernina Nappe occupied a more proximal position on the margin (Froitzheim & Manatschal 1996; Mohn et al. 2011).

From Middle Jurassic to Cretaceous times, stacking of the Austroalpine nappes was the result of the closure of the Meliata Ocean, southeast of Adria (Neubauer et al. 2000; Missoni & Gawlick 2011), and the following intracontinental shortening. This first orogenic event led to mainly W- to NW-directed thrusting. It was followed by the Eocene closure of the Penninic oceanic basins between Europe and Adria which resulted in the formation of the present day Penninic-Austroalpine nappe stack (Froitzheim et al. 1996; Müller et al. 1999). During this Early Tertiary collision, the

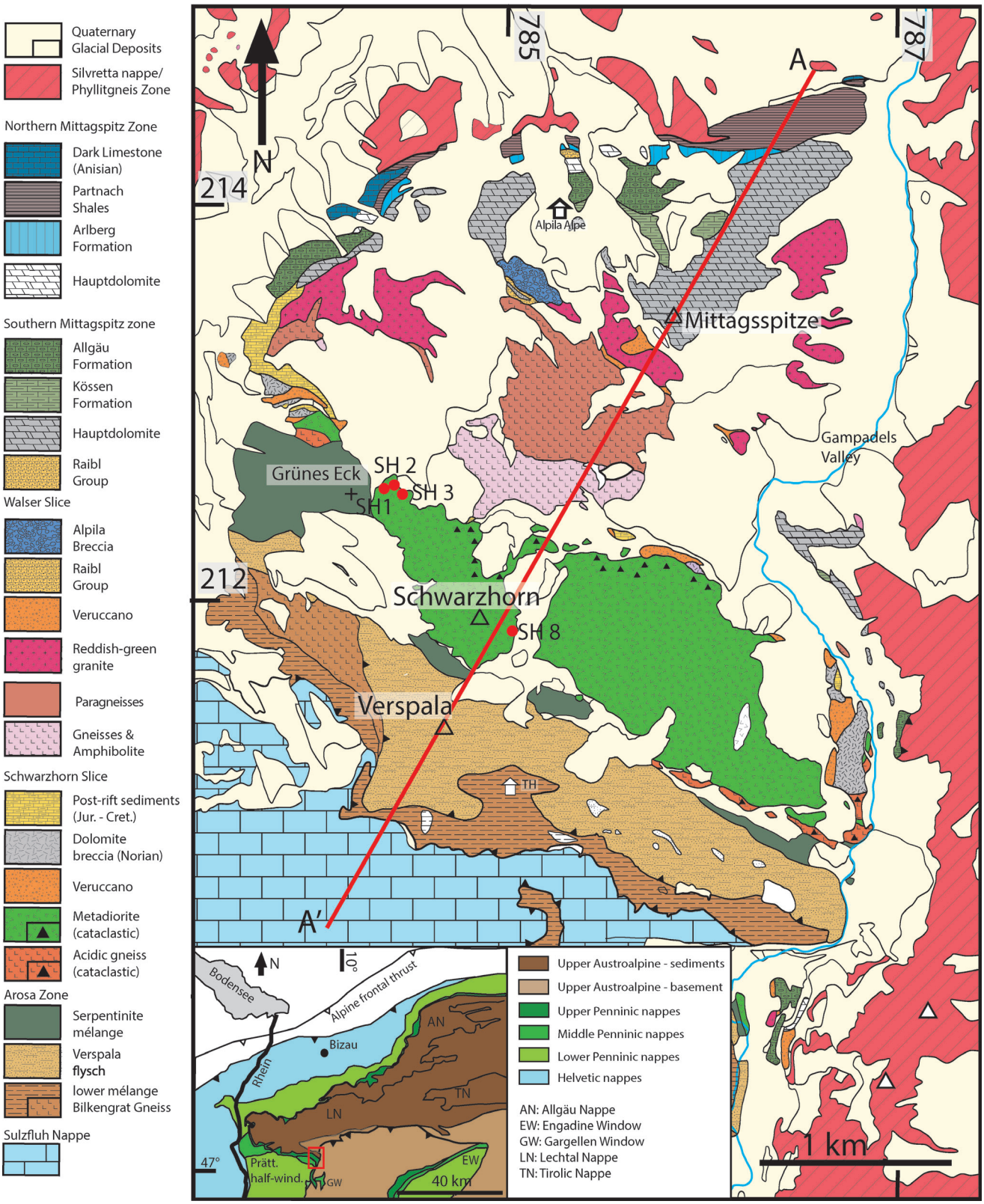

Fig. 1. Geological map of the Tilisuna area after Nagel (2006). Red dots with numbers indicate the sample localities. The inset in the lower left corner shows a geological sketch map of the north-western part of the Eastern Alps. Red frame indicates the map area.

Austroalpine nappes were thrust towards the north over the Penninic units (Ring et al. 1989; Froitzheim et al. 1994).

The nappe stack in the Tilisuna area

The Tilisuna area (Figs. 1 & 2) is characterized by a north-dipping nappe stack of Middle Penninic to Upper Austroalpine units, starting in the South with the Middle Penninic Sulzfluh Nappe (von Seidlitz 1906; Tollmann 1970; Burger 1978; Biehler 1990; Nagel 2006). It represents the sedimentary cover of the Briançonnais continental spur and comprises mainly Upper Jurassic platform carbonates, discordantly overlain by thin, often reddish, pelagic marls (Couches Rouges) of Late Cretaceous to Paleogene age (Allemann 1952).

To the north follows the Arosa Zone, comprising units derived from the Piemont-Ligurian Ocean. It is divided into three subunits, from bottom to top: (1) the lower mélange, consisting of a clay matrix with embedded slivers of Middle Penninic as well as Upper Austroalpine origin (von Seidlitz 1906; Stahel 1926); (2) the Cenomanian–Turonian Verspala flysch (Oberhauser 1983); (3) the upper mélange, comprising a matrix of mainly serpentinite and clasts of Upper Penninic and Lower Austroalpine origin (Nagel 2006).

To the North, the upper mélange is overlain by the ca. 4 km long and 1 km thick Schwarzhorn slice (Fig. 3). It follows the general SE–NW strike in the area from the Gampadels valley in the southeast to Grünes Eck in the northwest and builds the peak of Schwarzhorn (Fig. 1). The dominating lithology, making up two thirds of the Schwarzhorn slice, is the Schwarzhorn Amphibolite. The mineral composition reflects a dioritic to quartzdioritic magmatic predecessor which experienced amphibolite facies overprint. The fabric of the Schwarzhorn Amphibolite shows strong variations and reaches from strain-free domains where primary magmatic structures are preserved to amphibolites with a well-developed foliation. A pre-Mesozoic age of this metamorphism is indicated by the much lower, anchizonal overprint of the Mesozoic sedimentary cover (Ferreiro Mählmann & Giger 2012).

The sedimentary cover of the basement rocks is preserved on the northern and eastern margins of the Schwarzhorn slice. Despite the strong deformation, typical pre-, syn-, and post-rift sedimentary successions can be identified (Fig. 4). In the Gampadels valley, the cover of the meta-diorite starts with Scythian quartzites and sandstones, followed by dolomites and claystones of probably Late Triassic age (Nagel 2006). This pre-rift succession is discordantly overlain by strongly deformed Late Jurassic to Cretaceous post-rift sediments (von Seidlitz 1906; Furrer 1985). Sediments related to the syn-rift stage (Early to Middle Jurassic) are scarce. A small outcrop northeast of the Schwarzhorn shows a well bedded breccia with sedimentary components derived from the pre-rift sequence, and greenish granite components (Nagel 2006). The breccia rests on cataclastic basement rocks and is covered by post-rift sediments.

Along the northern and southeastern margins of the Schwarzhorn slice, two cataclastic fault zones are attributed to Jurassic rifting. Therefore the Schwarzhorn slice is interpreted as an eastward tilted block of the Jurassic passive margin, bounded by two westward dipping normal faults (Fig. 4) (Nagel 2006). Such faults are also known from the Lower Austroalpine Err Nappe further south (Eberli 1988; Froitzheim & Manatschal 1996). Based on these observations, Nagel (2006) attributed the Schwarzhorn slice to the Lower Austroalpine nappe system as formerly proposed by Cadisch (1923), while other authors treated it as part of the Arosa Zone (Richter 1958; Biehler 1990; Ferreiro Mählmann 1994).

The Walser slice overlies the Schwarzhorn slice and represents gneissic and granitic basement with remnants of Mesozoic cover. It is in a similar structural position as the Lower Austroalpine Bernina Nappe in SE Graubünden (Nagel 2006). The southern (SMZ) and the northern Mittagsspitz Zone (NMZ) follow to the north. They comprise Mesozoic sedimentary rocks. The SMZ is in a similar structural position as the Allgäu Nappe of the Northern Calcareous Alps, whereas the NMZ is connected with the Lechtal Nappe. The NMZ represents the inverted sediment cover of the Phyllit-gneiss Zone, a Variscan basement unit connected with the Silvretta Nappe.

Samples and analytical methods

Samples of Schwarzhorn Amphibolite were collected along the northwestern and the southern flank of the peak Schwarzhorn (Fig. 1). We sampled a representative suite to cover nearly undeformed, well foliated and catalastic domains respectively (Table 1). Petrological, geochemical and geochronological analyses were carried out at facilities of the Steinmann Institute, Bonn.

Rock samples were petrographically investigated by thin-section microscopy and electron-microprobe analysis (EMPA). The microprobe analyses of main and accessory minerals were carried out on a JEOL 8200 Superprobe. Whole rock major and trace element contents were measured by X-ray fluorescence (XRF) on $Li_2B_4O_7$-fluxed fusion discs (PANalytical-Axios spectrometer). Volatile-free mass proportions were recalculated to 100%.

For U-Pb zircon geochronology, a large aliquot of sample SH1 was crushed, milled and sieved before applying magnetic and heavy-liquid separation techniques. The processing of ca. 10 kg of meta-diorite yielded 407 zircon crystals. Optically clear, inclusion- and crack-free zircon was hand-picked under the binocular microscope and mounted in epoxy resin. After polishing down to half section, cathodoluminescence imaging was performed to reveal the internal textures. Established methods for U-Pb data acquisition (Kooijman et al. 2012) were adapted for application at the Steinmann facilities. Laser ablation inductively coupled plasma mass spectrometry (LA-ICP-MS) analyses were carried out using a Resonetics RESOlution M50-E 193nm excimer-laser coupled to a Thermo Scientific ELEMENT XR SF-ICP-MS. A comprehensive list of instrument settings and analytical strategy is provided in the online supplement (S1)*. In short, the gas blank was recorded for 27 seconds followed by the ablation for 30 seconds with a laser spot size of 33 μm

* Only in an electronical version on *www.geologicacarpathica.com*

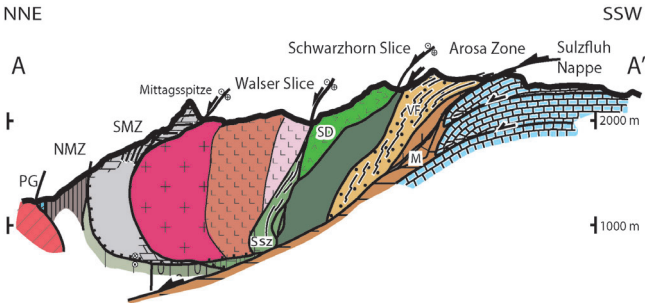

Fig. 3. The peak of Schwarzhorn, seen from the South. Dark rock at the base of the cliff is serpentinite (Arosa Zone). The cliff and the peak are meta-diorite. Light-coloured peak in the background to the right is Tschaggunser Mittagsspitze, formed by Upper Triassic Hauptdolomit of the Southern Mittagspitz Zone.

with 10 Hz repetition time and a fluency of 9 J/cm^2 . In order to avoid surface-related contamination, each spot was pre-ablated by three shots with a spot size of 58 µm. For laser-induced downhole fractionation, mass bias and instrument drift were corrected by normalizing to the 91500 zircon

Fig. 2. Cross section of the Tilisuna area after Nagel (2006). Lithology patterns are the same as in Fig.1. **M** — Lower and Upper Mélange; **NMZ** — Northern Mittagsspitz Zone; **PG** — Phyllit Gneiss; **SD** — Schwarzhorn Meta-Diorite; **SMZ** — Southern Mittagsspitz Zone; **Ssz** — Schwarzhorn shear zone; **VF** — Verspala Flysch.

Table 1: Overview of samples and interrelated analyses. Coordinates are given in Swiss Grid 1903 LV03.

Sample	Coordinates	Rock type	Analyses
SH1	E 784329 N 212557	moderately foliated amphibolite	LA-ICP-MS U-Pb, XRF
SH2	E 784330 N 212617	weakly foliated amphibolite	XRF
SH3	E 784350 N 212595	cataclastic amphibolite	XRF, EMPA
SH8	E 785037 N 211910	moderately foliated amphibolite	XRF, EMPA

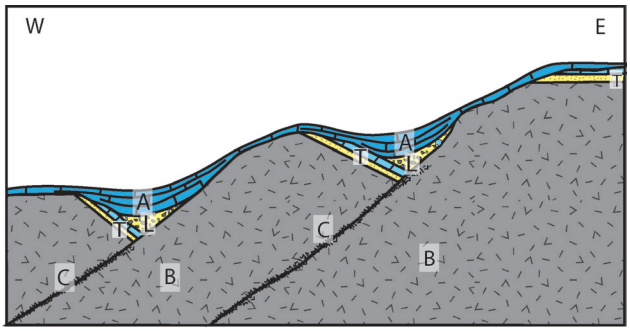

Fig. 4. Reconstructed cross-section of the Schwarzhorn slice after Early to Middle Jurassic rifting (Nagel 2006). **A** — post-rift sediments; **B** — dioritic basement (Schwarzhorn Amphibolite); **C** — rift-related cataclasites; **L** — syn-rift sediments; **T** — pre-rift sediments.

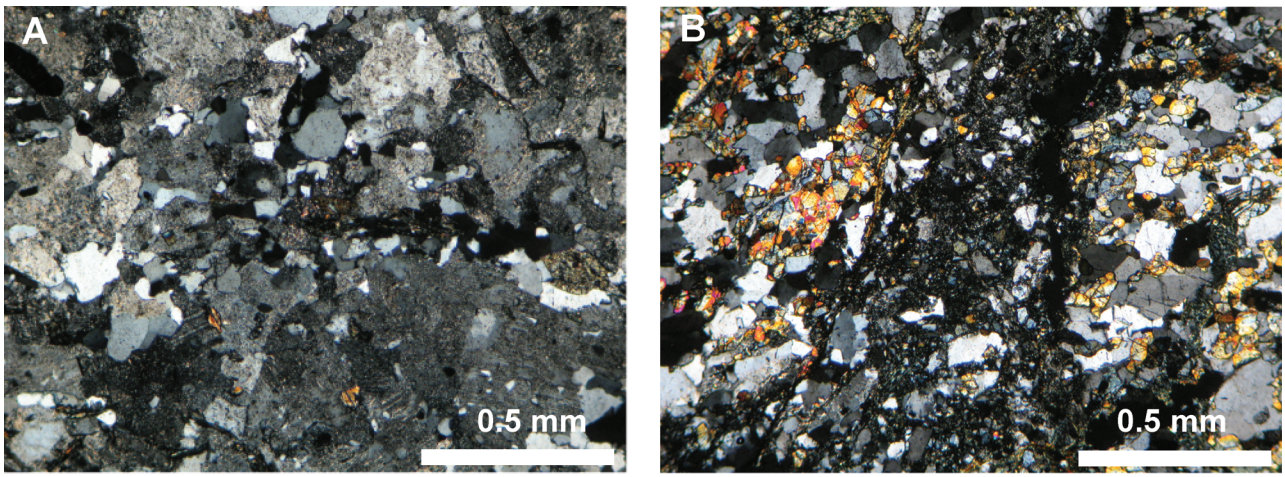

Fig. 5. A — Thin section micrograph of a moderately strained sample of the Schwarzhorn Amphibolite (SH1). **B** — Thin section micrograph of a cataclastic zone of sample SH3 with saussuritized plagioclase (XPL).

reference material (Wiedenbeck et al. 1995, 2004). Raw-data was processed using the reduction scheme VizualAge in Iolite 2.5 (Paton et al. 2011; Petrus & Kamber 2012). The stacking of measured signals in Iolite revealed an instability of element ratios during the first 6 seconds, and this time interval was excluded from data regression. Furthermore, a few reversely discordant analyses were rejected.

With correction for the monitored isobaric interference of ^{204}Hg on ^{204}Pb, the signal was indistinguishable from the background. The amount of common-Pb was generally found insignificant (f206<0.5 %), as expected for the given zircon free of inclusions or cracks, and no correction for common-Pb was applied. Within-run reproducibility of the primary reference material has been propagated into the final data, provided in Table 2. Data was plotted and population ages calculated with the help of the Isoplot plugin for Excel (Ludwig 2012). Concerning accuracy and systematic error estimation, the Plešovice zircon (online supplement S2, S4*) returned a concordia age of 339.6±1.7 Ma (internal error) which corresponds within an error of 1% to the accepted ID-TIMS age (337.13±0.37 Ma, Sláma et al. 2008). A systematic error of 1.5 % was propagated by quadratic addition into the final age of the unknown population.

Table 2: LA-ICP-MS U-Pb zircon data for Schwarzhorn Amphibolite sample SH1. (Sampling coordinates: E 784329, N 212563, Swiss Grid CH1903).

Analysis	Analysis	U	Th	Pb	^{206}Pb	^{238}U		Measured Isitopic Ratios							Ages [Ma]			
#	Name	[ppm]	[ppm]	[ppm]	[cps]	[cps]	f206%[a]	^{207}Pb/^{235}U	2σ	^{206}Pb/^{238}U	2σ	rho	^{207}Pb/^{206}Pb	2σ	^{207}Pb/^{235}U	2σ	^{206}Pb/^{238}U	2σ
3	**A2-1**	**154**	**27**	**7**	**101791**	**1005020**	**0,02**	**0,691**	**0,018**	**0,0853**	**0,0014**	**0,29**	**0,0581**	**0,0014**	**533**	**11**	**528**	**8**
4	**A4-1**	**163**	**36**	**9**	**108624**	**1060394**	**0,17**	**0,715**	**0,019**	**0,0864**	**0,0015**	**0,03**	**0,0595**	**0,0016**	**547**	**11**	**534**	**9**
5	**A6-1**	**108**	**17**	**5**	**72726**	**699785**	**0,05**	**0,713**	**0,025**	**0,0875**	**0,0019**	**0,40**	**0,0587**	**0,0019**	**546**	**15**	**541**	**11**
6	**A6-2**	**191**	**37**	**9**	**124990**	**1241142**	**0,11**	**0,696**	**0,023**	**0,0851**	**0,0015**	**0,22**	**0,0588**	**0,0018**	**536**	**14**	**526**	**9**
7	**A10-1**	**260**	**68**	**16**	**160118**	**1684224**	**0,10**	**0,691**	**0,021**	**0,0850**	**0,0015**	**0,59**	**0,0587**	**0,0019**	**533**	**13**	**526**	**9**
8	**A14-1**	**182**	**34**	**9**	**119063**	**1178368**	**0,06**	**0,692**	**0,022**	**0,0853**	**0,0016**	**0,12**	**0,0584**	**0,0018**	**534**	**13**	**528**	**9**
9	**A14-2**	**240**	**64**	**17**	**157383**	**1554820**	**0,12**	**0,705**	**0,021**	**0,0860**	**0,0016**	**0,05**	**0,0590**	**0,0017**	**541**	**13**	**532**	**9**
10	**A16-1**	**349**	**94**	**23**	**233913**	**2266224**	**-0,05**	**0,708**	**0,018**	**0,0875**	**0,0015**	**0,57**	**0,0579**	**0,0009**	**543**	**11**	**541**	**9**
14	**A21-1**	**148**	**37**	**9**	**96632**	**963624**	**0,00**	**0,686**	**0,027**	**0,0852**	**0,0015**	**0,41**	**0,0579**	**0,0020**	**529**	**16**	**527**	**9**
15	A21-2	190	58	14	129794	1240818	-0,22	0,688	0,018	0,0878	0,0015	0,38	0,0565	0,0012	531	11	542	9
16	A23-1	149	23	8	125803	975491	-0,07	0,928	0,040	0,1090	0,0032	0,34	0,0612	0,0021	665	21	667	19
17	**A24-1**	**171**	**44**	**10**	**113027**	**1120017**	**-0,06**	**0,682**	**0,020**	**0,0854**	**0,0014**	**0,16**	**0,0575**	**0,0015**	**527**	**12**	**528**	**8**
18	A24-2	533	84	20	362734	3511258	0,01	0,708	0,018	0,0876	0,0014	0,62	0,0584	0,0010	543	11	542	8
19	**B2-1**	**319**	**62**	**15**	**213538**	**2110332**	**0,07**	**0,693**	**0,018**	**0,0854**	**0,0014**	**0,56**	**0,0585**	**0,0011**	**534**	**11**	**528**	**9**
20	**B3-1**	**245**	**60**	**15**	**167897**	**1653688**	**0,15**	**0,701**	**0,033**	**0,0850**	**0,0026**	**0,51**	**0,0591**	**0,0024**	**539**	**20**	**526**	**15**
24	B9-1	297	41	10	184894	1998783	0,33	0,654	0,017	0,0794	0,0012	0,19	0,0597	0,0013	511	11	493	7
25	**B9-2**	**165**	**32**	**8**	**112077**	**1123529**	**-0,02**	**0,677**	**0,021**	**0,0846**	**0,0014**	**0,13**	**0,0577**	**0,0017**	**524**	**13**	**523**	**8**
26	**B10-1**	**241**	**56**	**14**	**163616**	**1641622**	**0,16**	**0,692**	**0,021**	**0,0844**	**0,0015**	**0,30**	**0,0591**	**0,0016**	**533**	**13**	**522**	**9**
27	**B17-1**	**129**	**26**	**6**	**89307**	**881753**	**-0,15**	**0,681**	**0,023**	**0,0863**	**0,0015**	**0,08**	**0,0569**	**0,0019**	**527**	**14**	**534**	**9**
28	B18-1	261	58	14	173084	1792597	0,06	0,667	0,019	0,0828	0,0020	0,45	0,0580	0,0015	518	12	512	12
29	B18-2	323	77	18	218249	2221950	0,17	0,683	0,018	0,0834	0,0016	0,13	0,0590	0,0017	528	11	517	10
30	**B24-1**	**203**	**51**	**13**	**140911**	**1403605**	**0,29**	**0,708**	**0,024**	**0,0854**	**0,0016**	**0,31**	**0,0603**	**0,0021**	**546**	**16**	**528**	**10**
34	B25-1	195	55	14	140549	1350262	-0,10	0,712	0,021	0,0890	0,0016	0,34	0,0577	0,0014	545	12	549	10
35	C2-1	325	46	11	208555	2249225	0,20	0,639	0,018	0,0787	0,0016	0,46	0,0585	0,0013	501	11	488	9
36	**C2-2**	**262**	**51**	**13**	**186185**	**1814030**	**-0,06**	**0,701**	**0,017**	**0,0875**	**0,0016**	**0,55**	**0,0578**	**0,0011**	**539**	**10**	**541**	**9**
37	**C10-1**	**251**	**58**	**14**	**175751**	**1736505**	**0,03**	**0,694**	**0,018**	**0,0859**	**0,0018**	**0,38**	**0,0583**	**0,0012**	**535**	**11**	**532**	**10**
38	C11-1	213	62	15	147916	1479372	0,32	0,684	0,026	0,0824	0,0016	0,32	0,0601	0,0021	529	16	510	9
39	**C11-2**	**207**	**62**	**15**	**142073**	**1431375**	**0,17**	**0,689**	**0,022**	**0,0846**	**0,0015**	**0,20**	**0,0592**	**0,0019**	**531**	**13**	**524**	**9**
40	**C11-3**	**448**	**68**	**15**	**307679**	**3107344**	**0,02**	**0,698**	**0,016**	**0,0863**	**0,0015**	**0,23**	**0,0583**	**0,0012**	**537**	**10**	**534**	**9**
44	C17-1	224	70	17	161215	1553728	-0,01	0,717	0,020	0,0885	0,0018	0,40	0,0584	0,0014	548	12	547	11
45	**C17-2**	**588**	**127**	**29**	**416099**	**4080341**	**-0,05**	**0,699**	**0,014**	**0,0871**	**0,0016**	**0,50**	**0,0578**	**0,0009**	**538**	**8**	**539**	**9**
46	C17-3	1000	193	44	726030	6949284	-0,10	0,713	0,014	0,0888	0,0016	0,49	0,0577	0,0009	547	8	548	9
47	**C20-1**	**209**	**59**	**14**	**145774**	**1453427**	**0,08**	**0,701**	**0,029**	**0,0859**	**0,0021**	**0,70**	**0,0587**	**0,0017**	**538**	**17**	**531**	**12**
48	C21-1	151	39	10	112705	1053666	-0,27	0,719	0,023	0,0913	0,0018	0,09	0,0567	0,0016	549	13	563	11
49	C30-1	145	37	9	110397	1012740	-0,06	0,753	0,021	0,0926	0,0014	0,13	0,0586	0,0015	570	12	571	8
50	C30-2	285	52	14	227132	1997377	-0,37	0,778	0,020	0,0984	0,0019	0,49	0,0570	0,0012	584	11	605	11
54	**D13-1**	**144**	**35**	**9**	**99907**	**1013060**	**0,27**	**0,716**	**0,025**	**0,0859**	**0,0018**	**0,51**	**0,0602**	**0,0017**	**548**	**15**	**531**	**11**
56	D16-1	164	38	10	121026	1147556	-0,02	0,727	0,024	0,0894	0,0015	0,06	0,0584	0,0019	554	14	552	9
57	**D16-2**	**537**	**81**	**19**	**374857**	**3771058**	**-0,10**	**0,669**	**0,013**	**0,0846**	**0,0015**	**0,24**	**0,0570**	**0,0010**	**520**	**8**	**523**	**9**
58	D25-1	207	64	17	159101	1453573	0,14	0,681	0,028	0,0885	0,0018	0,46	0,0596	0,0021	527	17	547	11
59	D25-2	255	41	11	217504	1796744	-0,40	0,805	0,019	0,1015	0,0019	0,16	0,0573	0,0013	599	10	623	11
60	D25-3	363	66	18	278781	2554336	-0,08	0,761	0,019	0,0937	0,0017	0,45	0,0586	0,0011	574	11	577	10
64	D25-4	949	209	46	641998	6678438	0,01	0,656	0,013	0,0823	0,0012	0,21	0,0576	0,0010	512	8	510	7
65	D26-1	240	70	17	178788	1688468	-0,18	0,730	0,023	0,0916	0,0020	0,43	0,0575	0,0015	556	14	565	12
66	**E12-1**	**254**	**69**	**16**	**174194**	**1787184**	**0,18**	**0,709**	**0,024**	**0,0858**	**0,0017**	**0,48**	**0,0595**	**0,0017**	**543**	**14**	**530**	**10**
67	E12-2	328	70	17	219082	2302962	0,08	0,662	0,017	0,0820	0,0017	0,41	0,0581	0,0012	515	10	508	10
68	E12-3	291	60	14	193126	2038157	0,33	0,678	0,021	0,0814	0,0018	0,58	0,0600	0,0015	525	13	504	11
69	**E15-1**	**218**	**61**	**14**	**153793**	**1523332**	**-0,15**	**0,693**	**0,026**	**0,0873**	**0,0018**	**0,56**	**0,0570**	**0,0016**	**534**	**15**	**539**	**11**
70	E15-2	216	37	9	151327	1508035	-0,06	0,707	0,026	0,0877	0,0023	0,46	0,0578	0,0018	542	16	542	14
74	**E16-1**	**182**	**42**	**10**	**128497**	**1260898**	**0,08**	**0,684**	**0,022**	**0,0845**	**0,0017**	**0,63**	**0,0585**	**0,0014**	**529**	**13**	**523**	**10**
75	**E16-2**	**750**	**93**	**22**	**528203**	**5182833**	**-0,04**	**0,701**	**0,014**	**0,0870**	**0,0014**	**0,35**	**0,0579**	**0,0009**	**539**	**9**	**538**	**8**
76	E18-1	276	88	22	197123	1898917	0,13	0,734	0,016	0,0882	0,0015	0,24	0,0595	0,0013	559	10	545	9

Bold marked analyses are used for age calculation by the TuffZirc algorithm.

[a]f206% denotes the fraction of ^{206}Pb that is common ^{206}Pb and is calculated with f206% = (^{207}Pb/^{206}Pb$_{measured}$ - ^{207}Pb*/^{206}Pb*) / (^{207}Pb/^{206}Pb$_{common}$ - ^{207}Pb*/^{206}Pb*)*100.

* Only in an electronical version on *www.geologicacarpathica.com*

Petrography and mineral chemistry

The meta-diorite of the Schwarzhorn slice mainly consists of hornblende, plagioclase and quartz as main constituents and rutile, epidote, apatite and rare zircon as accessory minerals. The textural range of meta-diorite samples comprises unstrained domains with preserved primary magmatic fabrics, domains with well-developed amphibolite-facies foliation, as well as cataclastic zones.

Unfoliated meta-diorite with a primary magmatic texture is characterized by large isometric plagioclase and hornblende. Plagioclase is strongly sericitizied and shows polysynthetic twinning. Zonation and twinning are also common in hornblende. It can be divided into core (hornblende 1) and rim domains (hornblende 2). The rims are yellow-greenish and show distinct pleochroism. The cores appear dark brown to almost opaque. Small inclusions of quartz and rutile are common in core domains but absent in rims. A magmatic amphibole composition is not directly preserved but high density of rutile inclusions indicates a Ti-rich precursor. Quartz veins and up to 1mm large grains make up ca. 10 % of the rock.

In moderately foliated rocks, plagioclase is completely recrystallized into smaller grains (Fig. 5a). The anorthitic component of plagioclase ranges from 10 % to 40 % (Table 3).With increasing foliation, the opaque and inclusion-rich core domains of hornblende 1 are replaced by inclusion-free, acicular grains of hornblende 2. All analysed amphiboles are magnesio-hornblende and no chemical distinction could be made between core and rim domains (Table 4). Chlorite and epidote interfinger with hornblende in rim domains (Fig. 6a).

In rocks with cataclastic overprint, hornblende is almost completely replaced by iron-rich chlorite. Brittle fault zones are characterized by fractured components of plagioclase and epidote and a phyllitic matrix of mainly chlorite, biotite (Phl_{31-55}) and some pumpellyite. Plagioclase shows common seritization and is the main constituent. It is recrystallized in grains of up to 0.3 mm size in unfractured domains. In brittle fault zones, the Ca-plagioclase has been altered to albite ($An_{0.2-12}$) (Fig. 7) and epidote (saussuritization) (Figs. 5b and 6b).

Whole-rock geochemistry

Results of XRF analyses of the Schwarzhorn Amphibolite are presented in Table 5 and Figure 8. The total alkali versus silica plot of Wilson (1989) indicates a dioritic composition of the protolith (Fig. 8a). A relatively large scatter of SiO_2 contents is observed and the composition ranges from SiO_2–poor diorite (55 wt. %) to quartz diorite (68 wt. %). According to the ternary diagram of Mullen (1983), all samples are within the island-arc tholeiite field, except for sample SH3 which plots due to its low TiO_2 content at the transition between island-arc tholeiite and calc-alkali basalt (Fig. 8b). A supra-subduction zone setting is also suggested by the Ti/Zr diagram of Pearce et al. (1982) where samples SH1, SH2, and SH8 reflect arc lava compositions (Fig. 8c). In the AFM diagram and the FeO^*/MgO vs. SiO_2 diagram, the Schwarzhorn Amphibolite shows a calc-alkaline differentiation trend (Fig. 8d, e).

Table 3: Representative electron microprobe analyses of feldspar in weight % oxides and molar proportions

	SH3		SH8									
Sample	**M9**	**M11**	**M7**	**M8**	**M9**	**M10**	**M11**	**M20**	**M21**	**M22**	**M23**	**M24**
SiO_2	71.32	66.86	59.47	61.82	58.01	61.94	58.34	57.99	58.48	66.47	58.14	64.10
TiO_2	0.00	0.00	0.00	0.00	0.01	0.00	0.00	0.00	0.02	0.01	0.01	0.05
Al_2O_3	19.97	22.01	25.86	24.22	26.51	23.93	26.57	26.76	26.79	21.73	26.52	23.46
FeO	0.03	0.03	0.00	0.00	0.01	0.02	0.02	0.01	0.06	0.00	0.05	0.00
MnO	0.00	0.00	0.00	0.04	0.00	0.02	0.00	0.03	0.00	0.00	0.02	0.00
MgO	0.00	0.00	0.02	0.00	0.00	0.03	0.00	0.00	0.01	0.00	0.00	0.01
CaO	0.08	2.75	7.25	5.50	8.32	5.44	8.34	8.58	8.41	2.56	8.55	4.60
Na_2O	10.39	10.18	7.07	8.28	6.81	8.08	6.85	6.66	6.72	10.04	6.52	8.78
K_2O	0.12	0.12	0.09	0.09	0.05	0.12	0.06	0.07	0.06	0.08	0.08	0.12
Cr_2O_3	0.00	0.00	0.03	0.01	0.00	0.01	0.00	0.00	0.01	0.00	0.00	0.01
Total	101.91	101.94	99.79	99.96	99.72	99.57	100.19	100.10	100.56	100.90	99.87	101.11
Orthoclase	0.69	0.64	0.53	0.52	0.30	0.67	0.36	0.38	0.36	0.46	0.45	0.68
Anorthite	0.22	12.37	35.74	26.57	40.09	26.05	39.91	41.18	40.48	11.82	40.84	21.43
Albite	99.09	86.99	63.73	72.91	59.60	73.28	59.73	58.44	59.16	87.72	58.71	77.89

Table 4: Representative electron microprobe analyses of amphibole in weight % and cations p.f.u.

	SH8									
Sample	**M1**	**M2**	**M3**	**M13**	**M14**	**M15**	**M16**	**M17**	**M18**	**M28**
SiO_2	45.31	45.65	43.46	45.25	45.84	48.01	46.19	43.69	44.94	44.48
TiO_2	0.49	0.49	0.54	0.45	0.48	0.36	0.51	0.49	0.51	0.47
Al_2O_3	12.86	12.69	14.50	13.38	12.76	10.77	12.21	15.78	14.26	14.61
FeO	12.11	12.22	13.00	12.61	12.26	11.55	12.32	13.46	12.86	12.99
MnO	0.32	0.27	0.23	0.22	0.12	0.23	0.25	0.24	0.23	0.23
MgO	12.91	12.48	11.48	12.35	12.69	13.86	12.84	11.16	11.94	11.48
CaO	11.66	11.70	11.66	11.65	11.91	11.62	11.57	11.51	11.48	11.96
Na_2O	1.39	1.28	1.48	1.36	1.20	1.16	1.36	1.63	1.41	1.27
K_2O	0.28	0.32	0.37	0.39	0.26	0.30	0.27	0.40	0.29	0.29
Cr_2O_3	0.06	0.03	0.06	0.10	0.05	0.03	0.08	0.08	0.00	0.01
Total	97.05	96.79	96.34	97.25	97.25	97.56	97.24	97.94	97.62	97.48
Cations p.f.u.										
Si	6.60	6.66	6.42	6.58	6.66	6.91	6.71	6.35	6.52	6.48
Ti	0.05	0.05	0.06	0.05	0.05	0.04	0.06	0.05	0.06	0.05
Al	2.21	2.18	2.52	2.29	2.18	1.83	2.09	2.70	2.44	2.51
Fe	1.48	1.49	1.61	1.53	1.49	1.39	1.50	1.63	1.56	1.58
Mn	0.04	0.03	0.03	0.03	0.01	0.03	0.03	0.03	0.03	0.03
Mg	2.81	2.72	2.53	2.68	2.75	2.97	2.78	2.42	2.58	2.49
Ca	1.82	1.83	1.84	1.82	1.85	1.79	1.80	1.79	1.78	1.87
Na	0.39	0.36	0.42	0.38	0.34	0.32	0.38	0.46	0.40	0.36
K	0.05	0.06	0.07	0.07	0.05	0.05	0.05	0.07	0.05	0.05
Cr	0.01	0.00	0.01	0.01	0.01	0.00	0.01	0.01	0.00	0.00
Total (f.p 23 O^2)	15.45	15.40	15.50	15.43	15.38	15.33	15.39	15.50	15.42	15.42

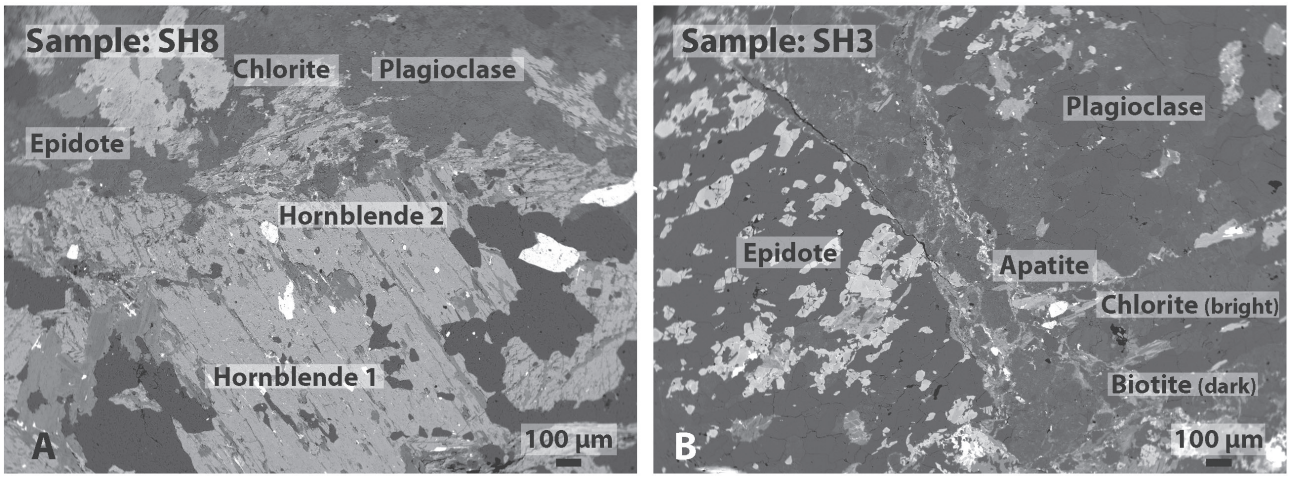

Fig. 6. Backscattered electron images of the Schwarzhorn Amphibolite. **A** — Moderately foliated amphibolite with hornblende 1 and rim of hornblende 2. **B** — Plagioclase of the cataclastic sample SH3 shows saussuritization. Amphibole is replaced by chlorite.

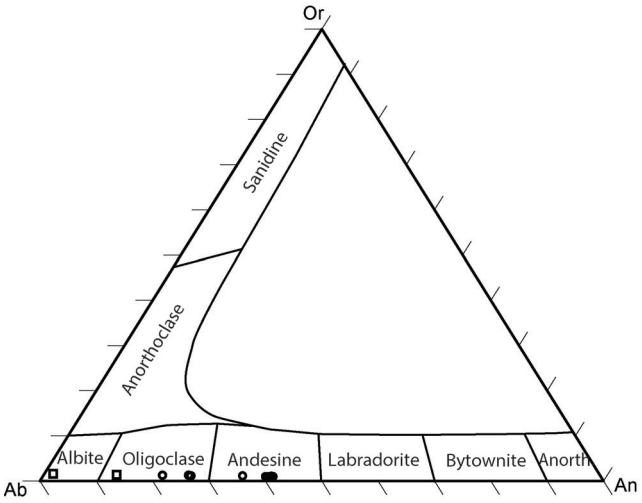

Fig. 7. Results of feldspar microprobe analyses. Rectangles reflect analyses from cataclastic rock units and indicate that plagioclase has been altered to a more albitic composition. Dots reflect analyses from the moderately foliated sample SH8.

Zircon U-Pb geochronology

The zircon crystals of the Schwarzhorn Amphibolite appear under the binocular microscope inclusion free and mostly colourless, some are slightly yellowish. The size of the zircons ranges from 50 to 200 µm. Grains show typically a short to medium prismatic morphology with a width-to-length ratio of 1:1 to 1:2, and rarely 1:3. Crystal faces are mostly subhedrally developed. CL images (Fig. 9) reveal that the internal texture is dominated by broad oscillatory zoning patterns as typically found in zircons precipitated from melts (e.g. Corfu et al. 2003). Oscillatory domains are commonly surrounded by a thin (1 to 5 µm) bright-CL rim discordantly crosscutting oscillatory zoning patterns (Fig. 9).

The results of the U-Pb analyses of the Schwarzhorn Amphibolite are listed in Table 2 and shown in Figure 10. Single spot $^{206}Pb/^{238}U$ ages range between ca. 488 and 667 Ma with a main population at about 530 Ma. Multiple spot analyses of rim and core domains of single zircon grains either did not yield satisfactory results or did not comprise significant age

Table 5: Major- and trace-element analyses of Schwarzhorn Amphibolite. Oxides are in [wt. %].

Sample	SH1	SH2	SH3	SH8
SiO_2	60,01	62,89	68,71	54,27
Al_2O_3	16,49	15,42	13,35	17,20
Fe_2O_3	6,96	5,76	4,18	7,10
MnO	0,14	0,09	0,07	0,13
MgO	4,05	4,08	2,31	6,92
CaO	3,18	2,32	3,66	6,04
Na_2O	3,90	4,90	3,57	3,40
K_2O	1,07	0,92	0,77	0,88
TiO_2	0,42	0,61	0,21	0,59
P_2O_5	0,06	0,11	0,05	0,08
SO_3	0,04	0,06	0,03	0,03
L.O.I.	2,95	2,70	2,21	2,53
Sum	99,27	99,86	99,12	99,17
Mg#[a)]	54	58	52	66
Trace Elements (ppm)				
As	-	2	3	3
Ba	190	110	129	110
Ce	8	16	20	16
Co	16	16	8	26
Cr	53	55	47	164
Cs	-	-	4	-
Cu	17	37	18	31
Ga	14	13	13	16
Hf	1	2	-	-
La	16	18	10	23
Mn	>1000	628	483	920
Mo	-	-	-	-
Nb	1	3	-	2
Nd	4	7	9	6
Ni	15	18	10	57
Pb	12	15	18	14
Rb	34	22	20	21
Sc	21	17	11	23
Sm	0	4	2	1
Sr	274	192	333	407
Th	2	3	3	2
U	2	4	4	3
V	107	112	55	159
W	17	12	10	19
Y	15	17	11	9
Zn	64	54	33	84
Zr	44	86	44	44

[a)] Mg# = (MgO/MgO+FeO)*100

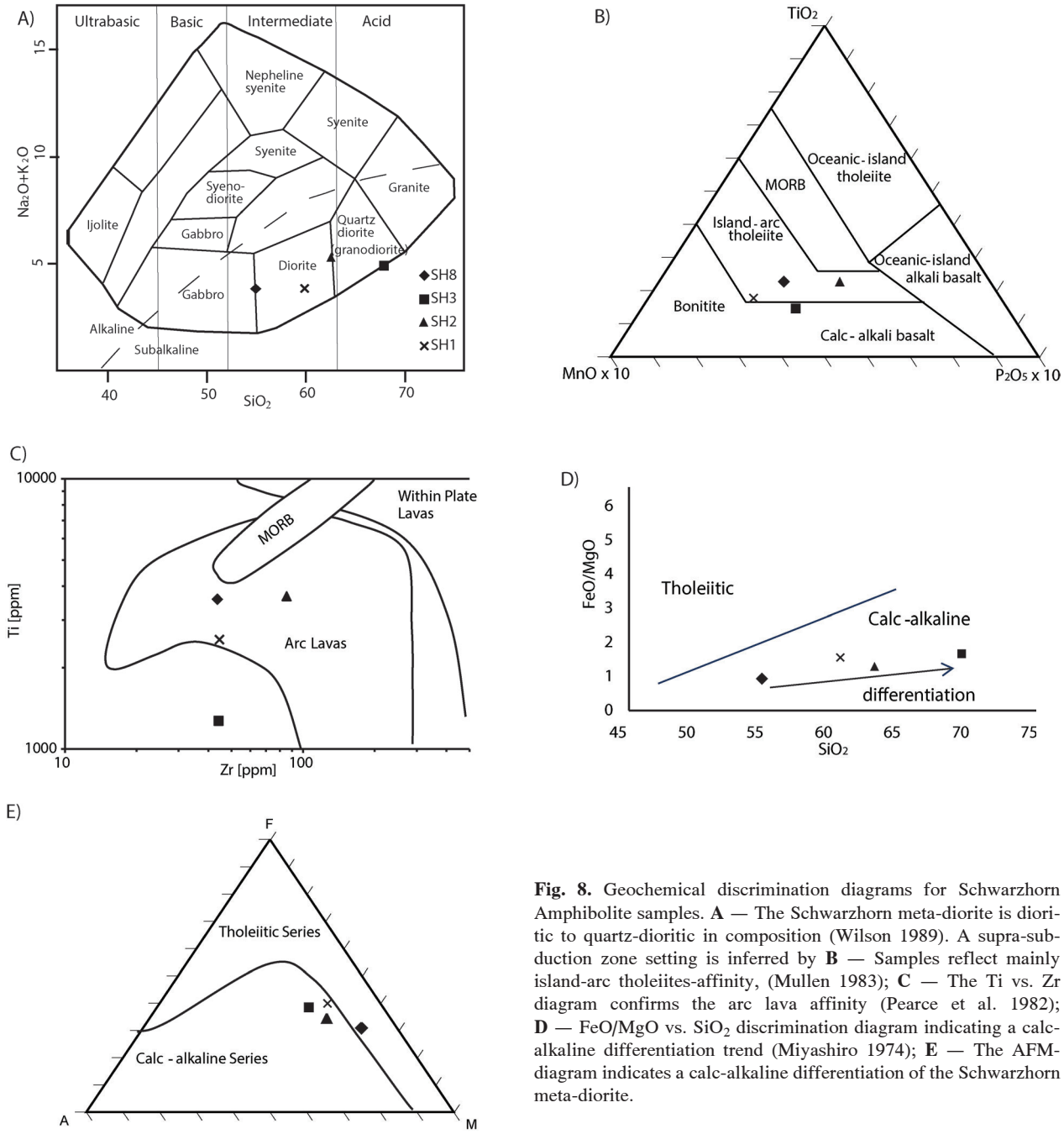

Fig. 8. Geochemical discrimination diagrams for Schwarzhorn Amphibolite samples. **A** — The Schwarzhorn meta-diorite is dioritic to quartz-dioritic in composition (Wilson 1989). A supra-subduction zone setting is inferred by **B** — Samples reflect mainly island-arc tholeiites-affinity, (Mullen 1983); **C** — The Ti vs. Zr diagram confirms the arc lava affinity (Pearce et al. 1982); **D** — FeO/MgO vs. SiO_2 discrimination diagram indicating a calc-alkaline differentiation trend (Miyashiro 1974); **E** — The AFM-diagram indicates a calc-alkaline differentiation of the Schwarzhorn meta-diorite.

Table 6: Compilation of U-Pb zircon ages for older orthogneisses.

Unit	Method	Age (Ma)	Inferred Tectonic Setting	Reference
Meta-diorite, Val Lavinouz	TIMS	609±3	Diorite - island arc	Schaltegger et al. (1997)
Biotite-hornblende gneiss, Val Lavinuoz	TIMS	568±6	Basic to intermediate igneous rock - island arc	Müller et al. (1995)
Quartz bearing Meta-Gabbro, Val Barlas	TIMS	537±4	Tholeiitic Island Arc basalt	Poller (1997)
Biotite-plagioglase gneiss	Pb-Pb evaporation	533±4	calc-alcaline protolith	Müller et al. (1995)
Garnet-hornblende-plagioclase gneiss, Val Sarsura	TIMS	532±30	Back-arc or fore-arc basin	Müller et al. (1996)
Schwarzhorn Amphibolite, Tilisuna Area	LA-ICPMS	529+9/–8	Diorite - supra-subduction zone	present study
Mönchalp gneiss, Val Barlas	TIMS	528±4	S-type granite - island arc or back-arc	Poller (1997)
K-feldspar gneiss, Val Lavinouz	TIMS	526±7	Alkaline s-type granite - supra-subduction zone	Müller et al. (1995)
Meta-tonalite, Val Sarsura	TIMS	524±6	Island arc	Schaltegger et al. (1997)
Flasergabbro, Val Sarsura	TIMS	523±3	Island arc	Schaltegger et al. (1997)
Coarse-grained meta-gabbro, Val Sarsura	TIMS	522±6	Island arc	Schaltegger et al. (1997)

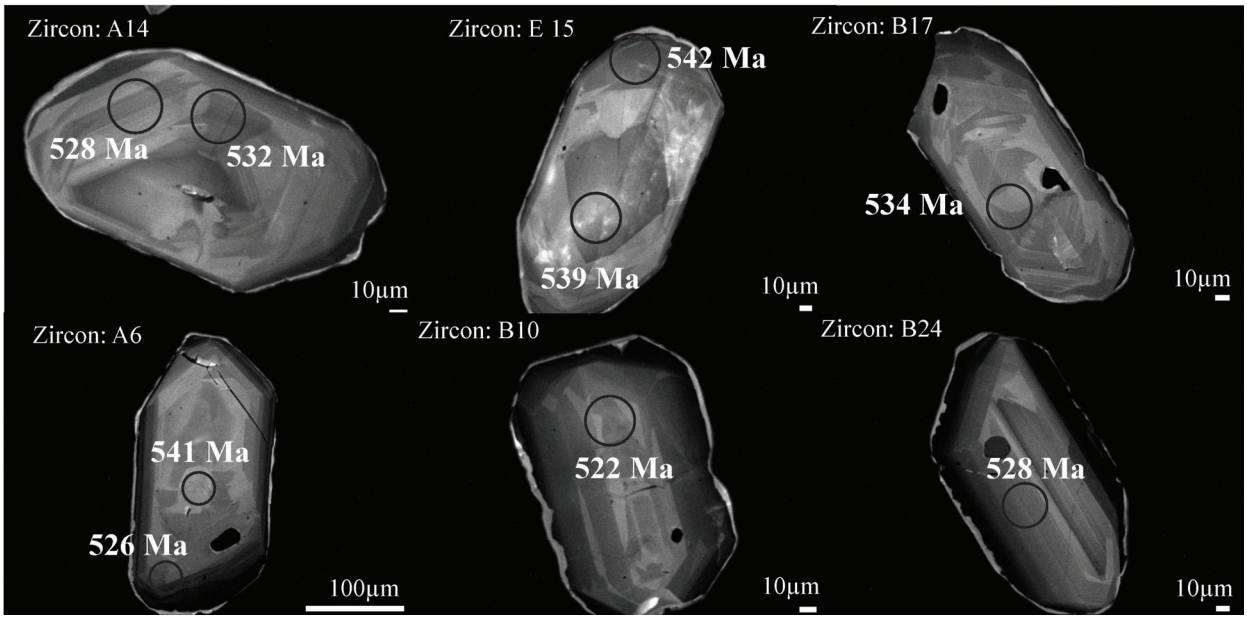

Fig. 9. CL-images of representative zircon crystals and location of LA-ICP-MS analyses. Zoning patterns are characterized by well-developed magmatic growth zoning and a surrounding thin high-CL rim. Numbers give single spot $^{206}Pb/^{238}U$ -ages (Table 2).

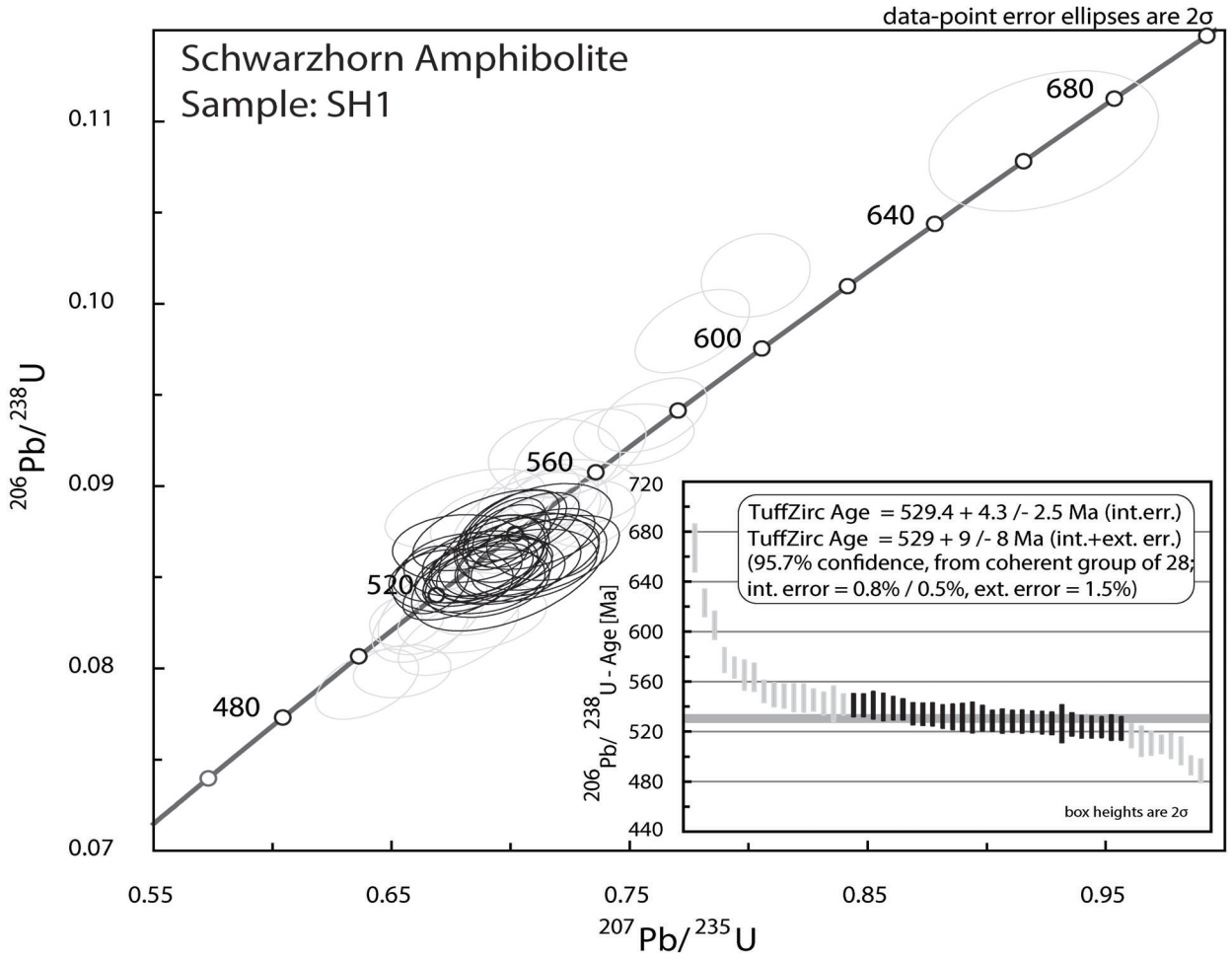

Fig. 10. Results of U-Pb zircon isotopic analysis. The protolith age is calculated with the black marked analyses of the *TuffZircAge* population (inset).

differences. Whereas the oldest age indicates some inheritance, the youngest ages tend to be discordant (Fig. 10) and hence are interpreted as influenced by lead-loss during a later tectono-thermal event.

The large scatter of the dates, in combination with a relatively continuous distribution between minimum and maximum ages (Fig. 10), impedes the selection of a population which represents the protolith age of the intrusion. To prevent a subjective bias of the population, we used the *TuffZirc* algorithm of Ludwig and Mundil (2002). It primarily excludes analyses with anomalously high errors and seeks to find a representative population of ranked $^{206}Pb/^{238}U$ dates which yield a probability of fit >0.05. The medium age of this population is reported with an asymmetric 95% confidence error. The resulting population consists of 28 analyses with a $^{206}Pb/^{238}U$-age of 529+9/–8 Ma (Fig. 10 inset).

Discussion

Whole rock geochemical and U-Pb zircon geochronological analyses of the Schwarzhorn Amphibolite reveal that the protolith formed in a supra-subduction zone setting (Fig. 8b–e) in the Early Cambrian. Meta-magmatic rocks of Neoproterozoic to Ordovician age are commonly found in Alpine basement units and are attributed to an active margin setting north of Gondwana. In the Austroalpine, pre-Variscan magmatites are reported from meta-gabbros in the Ötztal basement with 530–521 Ma reflecting MORB affinity (Miller & Thöni 1995) and from basement units south of the Tauern Window with 590–450 Ma (Schulz et al. 2004; Schulz 2008). Neoproterozoic to Cambrian intrusives of the latter, rather reflect subduction related magmatism, whereas Ordovician magmatites are characterized by acid magmatism from crustal sources. An early stage of an active margin setting is attributed to a 590 Ma N-MORB-type basite, which is followed by more abundant volcanic arc basalts of early Cambrian age (Schulz et al. 2004). Similarly, the Silvretta Nappe was divided into the Neoproterozoic to Lower Cambrian "older orthogneiss" and the Ordovician "younger orthogneiss" (Maggetti & Flisch 1993; Poller 1997; Müller et al. 1994, 1995, 1996). Thus, the protolithic age of 529+9/–8 Ma of the Schwarzhorn Amphibolite would correspond to rock units regarded as "older orthogneisses" or "gneiss-amphibolite complexes". Although older orthogneisses summarize a heterogeneous group of rock units, ranging from granitic through intermediate to mafic and ultra-mafic gneisses and amphibolites, they are geochemically characterized by a calc-alkaline affinity. In contrast, younger othogneisses show a more alkaline affinity. The reported intrusion ages of older orthogneisses (Table 6) indicate two phases of increased magmatic activity in the Late Proterozoic and Early Cambrian, related to a complex active margin setting on the northern margin of Gondwana (von Quadt 1992; Kounov et al. 2012; von Raumer et al. 2003, 2013). The first evidence of island arc magmatism is given by the 609±3 Ma metadiorite and a 568±6 Ma calc-alkaline orthogneiss (Schaltegger et al. 1997; Müller et al. 1995). Between 535 Ma and 520 Ma, oceanic plagiogranites infer the evolution of either back-arc or fore-arc basins but also contemporary island arc magmatism, as indicated by tholeiitic island arc basalts, calc-alkaline intermediate rocks and an S-type granitoid (Müller et al. 1995, 1996; Poller 1997; Schaltegger et al. 1997). This is in accordance with the geochemical characteristics of the Schwarzhorn Amphibolite which suggest a supra-subduction zone setting, and in this context most probably in an island arc setting. Subsequently the Neoproterozoic to Cambrian back arc or fore arc basins were closed and the island arc and micro-continents at the Gondwana margin were involved into an Ordovician to Silurian orogeny as indicated by S-type granitoids and gabbroic intrusions in a collisional belt, namely the "younger orthogneiss units"(Liebetrau 1996; Poller 1997).

The dominant amphibolite facies overprint (M1) of the Schwarzhorn meta-diorite may be either related to a vaguely constrained high-pressure event between 470 Ma and 530 Ma suggested by Poller (1997), or more probably to the Variscan orogenic cycle. Ladenhauf et al. (2001) dated metamorphic domains in zircons from eclogite of the Silvretta nappe at 351±22 Ma (U-Pb SHRIMP), similar to Sm-Nd isochrons for eclogites of the Ötztal basement (Miller & Thöni 1995). Unfortunately, the bright-Cl "metamorphic rims", crosscutting the growth-zoned Schwarzhorn metadiorite zircons, were too narrow for conventional LA-ICP-MS analyses.

Cataclastic zones of the Schwarzhorn Amphibolite comprise a low-temperature greenschist-facies mineral assemblage (M2). This is expressed by the lack of biotite, the alteration of Ca-plagioclase to albite and epidote and the replacement of amphibole by iron-rich chlorite. Coal and clay petrological studies have demonstrated that Alpine metamorphism did not exceed high-grade diagenetic conditions in the Tilisuna area (Ferreiro Mählmann & Giger 2012). Hence, we interpret the cogenetic low-temperature greenschist facies metamorphism and cataclastic faulting as a reflection of Jurassic rifting.

We note that the preservation of rift-related structures clearly indicates that the Schwarzhorn slice is part of the Lower Austroalpine nappe system (Nagel 2006). While "older orthogneisses" are particularly well documented from the Upper Austroalpine, the Cambrian protolith age of the Schwarzhorn Amphibolite provides the first evidence for the presence of similar rocks in the Lower Austroalpine. To date, the rare geochronological data from the Lower Austroalpine basement rocks comprises mostly Paleozoic ages linked to Variscan tectonics, which intruded in a poly-metamorphic basement (von Quadt et al. 1994). Great petrological and geological similarities between the Schwarzhorn Amphibolite and the southward located "Gabbrozug Arosa-Davos-Klosters" (Streckeisen 1948) of the Lower Austroalpine Dorfberg Nappe suggest a similar age of the Dorfberg Nappe basement.

Conclusion

1. U-Pb zircon geochronology of the Schwarzhorn Amphibolite yields a magmatic protolith age of 529+9/–8 Ma.

2. The magmatic precursor of the Schwarzhorn Amphibolite formed in a supra-subduction zone setting at the northern margin of Gondwana.

3. The rock is part of the Variscan basement of the Lower Austroalpine with close similarities to the Upper Austroalpine "older orthogneiss" of the Silvretta Nappe.

4. It became a tilted fault block of the distal passive margin during Jurassic rifting, and was incorporated in an imbricate stack of tectonic slivers during Cretaceous and Tertiary thrusting.

Acknowledgements: The authors would like to thank Nils Jung for the careful preparation of thin sections and sample mounts. Further, Radegund Hoffbauer and Kathrin Faßmer are thanked for XRF analysis, and Jiří Sláma for providing a split of the Plešovice zircon reference material. Finally, the authors gratefully appreciate the constructive reviews of Jürgen von Raumer and Albrecht von Quadt, which were a great help. This is contribution No. 28 from the DFG-funded LA-ICP-MS laboratory of the Steinmann-Institut Bonn.

References

Allemann F. 1952: Die Couches Rouges der Sulzfluhdecke im Fürstentum Liechtenstein. *Eclogae Geol. Helv.* 45, 264–298.

Biehler D. 1990: Strukturelle Entwicklung der Penninisch-Ostalpinen Grenzzone am Beispiel der Arosa Zone im Ost-Rätikon (Vorarlberg, Österreich). *Eclogae Geol. Helv.* 83, 221–239.

Burger H. 1978: Arosa- und Madrisa-Zone im Gebiet zwischen Schollberg und Verspala (Osträtikon). *Eclogae Geol. Helv*. 71, 255–266.

Cadisch J. 1923: Geologie der Weissfluhgruppe. *Beitr. Geol. Karte der Schweiz NF 49*, 50.

Corfu F., Hanchar J.M., Hoskin P. & Kinny P. 2003: Atlas of zircon textures. In: Hanchar J.M. & Hoskin P.W.O. (Eds.): Zircon. *Rev. Mineral. Geochem*. 53, 469–500.

Eberli G.P. 1988: The evolution of the southern continental margin of the Jurassic Tethys ocean as recorded in the Allgäu Formation of the Austroalpine Nappes of Graubünden (Switzerland). *Eclogae Geol. Helv.* 81, 175–214.

Ferreiro Mählmann R. 1994: Zur Bestimmung von Diagenesehöhe und beginnender Metamorphose-Temperaturgeschichte und Tektogenese des Austroalpins und Südpenninikums in Vorarlberg und Mittelbünden. *Frankfurter Geowiss. Arb.* C14, 1–498.

Ferreiro Mählmann R. & Giger M. 2012: The Arosa zone in Eastern Switzerland: oceanic, sedimentary burial, accretional and orogenic very low- to low-grade patterns in a tectono-metamorphic mélange. *Swiss. J. Geosci.* 105, 203–233.

Froitzheim N. & Eberli G. 1990: Extensional detachment faulting in the evolution of a Tethys passive continental margin, Eastern Alps, Switzerland. *Geol. Soc. Amer. Bull.* 102, 1297–308.

Froitzheim N. & Manatschal G. 1996: Kinematics of Jurassic rifting, mantle exhumation, and passive-margin formation in the Austroalpine and Penninic nappes (eastern Switzerland). *Geol. Soc. Amer. Bull.* 108, 1120–1133.

Froitzheim N., Schmid S.M. & Conti P. 1994: Repeated change from crustal shortening to orogen-parallel extension in the Austroalpine units of Graubünden. *Eclogae Geol. Helv.* 87, 559–612.

Froitzheim N., Schmid S.M. & Frey M. 1996: Mesozoic paleogeography and the timing of eclogite facies metamorphism in the Alps: a working hypothesis. *Eclogae Geol. Helv.* 89, 81–110.

Furrer H. 1985: Field workshop on Triassic and Jurassic sediments in the Eastern Alps of Switzerland. *Mitt. Geol. Inst. ETH Zürich* 248, 1–81.

Handy M.R. 1996: The transition from passive to active margin tectonics: a case study from the Zone of Samedan (eastern Switzerland). *Geol. Rundsch.* 85, 832–851.

Kooijman E., Berndt J. & Mezger K. 2012: U-Pb dating of zircon by laser ablation ICP-MS: recent improvements and new insights. *Eur. J. Mineral.* 24, 5–21.

Kounov A., Graf J., von Quadt A., Bernoulli D., Burg J.P., Seward D., Ivanov Z. & Fanning M. 2012: Evidence for a "Cadomian" ophiolite and magmatic-arc complex in SW Bulgaria. *Gondwana Res.* 212–213, 257–295.

Ladenhauf C., Armstrong R.A., Konzett J. & Miller C 2001: The timing of the pre-alpine HP-metamorphism in the Eastern Alps: constraints from U-Pb SHRIMP dating of eclogite zircons from the Austro-Alpine Silvretta nappe. *Geol. Paläont. Mitt. Innsbruck*. 25, 131.

Liebetrau V. 1996: Petrographie, Geochemie und Datierung der "Flüelagranitischen Assoziation" (sog. Jüngere Orthogneise) des Silvrettakristallins, Graubünden — Schweiz. *Dissertation University Freiburg (Switzerland)*, 1–233.

Ludwig K.R. 2012: Isoplot 3.75. A geochronological toolkit for Microsoft Excel. *Berkeley Geochronology Center Spec. Publ.* 5, 1–75.

Ludwig K.R. & Mundil R. 2002: Extracting reliable U-Pb ages and errors from complex populations of zircons from Phanerozoic tuffs. *Geochim. Cosmochim. Acta* 66, Supplement 1, 463.

Maggetti M. & Flisch M. 1993: Evolution of the Silvretta Nappe. In: von Raumer J.F. & Neubauer F. (Eds.): Pre-mesozoic geology in the Alps. *Springer*, Berlin, 469–484.

Miller C. & Thöni M. 1995: Origin of eclogites from the Austroalpine Ötztal basement (Tirol, Austria): geochemistry and Sm-Nd vs. Rb-Sr isotope systematics. *Chem. Geol.* 122, 199–225.

Missoni S. & Gawlick H.J. 2011: Jurassic mountain building and Mesozoic-Cenozoic geodynamic evolution of the Northern Calcareous Alps as proven in the Berchtesgaden Alps (Germany). *Facies* 57, 137–186.

Miyashiro A. 1974: Volcanic rock series in island arcs and active continental margins. *Amer. J. Sci*. 274, 321–355.

Mohn G., Manatschal G., Müntener O., Beltrando M. & Masini E. 2010: Unravelling the interaction between tectonic and sedimentary processes during lithospheric thinning in the Alpine Tethys margins. *Int. J. Earth Sci.* 99, 75–101.

Mohn G., Manatschal G., Masini E. & Müntener O. 2011: Rift-related inheritance in orogens: a case study from the Austroalpine nappes in Central Alps (SE-Switzerland and N-Italy). *Int. J. Earth Sci.* 100, 937–961.

Mullen E.D. 1983: $MnO/TiO_2/P_2O_5$: a minor element discriminant for basaltic rocks of oceanic environments and its implications for petrogenesis. *Earth Planet. Sci. Lett.* 62, 53–62.

Müller B., Klötzli U. & Flisch M. 1994: Dating of the Silvretta Older Orthogneiss intrusion: U-Pb-zircon data indicate cadomian magmatism in the Upper Austroalpine realm. *J. Czech Geol. Soc*. 39, 74–75.

Müller B., Klötzli U. & Flisch M. 1995: U-Pb and Pb-Pb zircon dating of the older orthogneiss suite in the Silvretta nappe, eastern Alps: Cadomian magmatism in the upper Austro-Alpine realm. *Geol. Rundsch.* 84, 457–465.

Müller B., Klötzli U.S., Schaltegger U. & Flisch M. 1996: Early Cambrian oceanic plagiogranite in the Silvretta Nappe, eastern Alps: geochemical, zircon U-Pb and Rb-Sr data from garnet-hornblende-plagioclase gneisses. *Geol. Rundsch*. 85, 822–831.

Müller W., Dallmeyer R.D., Neubauer F. & Thöni M. 1999: Deformation-induced resetting of Rb/Sr and $^{40}Ar/^{39}Ar$ mineral sys-

tems in a low-grade, polymetamorphic terrane (eastern Alps, Austria). *J. Geol. Soc. London* 156, 261–278.

Nagel T. 2006: Structure of Austroalpine and Penninic units in the Tilisuna area (Eastern Rätikon, Austria): implications for the paleogeographic position of the Allgäu and Lechtal nappes. *Eclogae Geol. Helv*. 99, 223–235.

Neubauer F., Genser J. & Handler R. 2000: The Eastern Alps: Result of a two-stage collision process. *Mitt. Österr. Geol. Ges.* 92, 117–134.

Oberhauser R. 1983: Mikrofossilfunde im Nordwestteil des Unterengadiner Fensters sowie im Verspalaflysch des Rätikon. *Jb. Geol. Bundesanst. Wien* 126, 71–93.

Paton C., Hellstrom J., Paul B., Woodhead J. & Hergt J. 2011: Iolite: Freeware for the visualisation and processing of mass spectrometric data. *J. Anal. Atom. Spectrometry* 26, 2508–2518.

Pearce J.A. 1982: Trace element characteristics of lavas from destructive plate boundaries. In: Thorpe R.S. (Ed.): Andesites: Orogenic Andesites and Related Rocks. *John Wiley & Sons*, 525–548.

Petrus J.A. & Kamber B.S. 2012: VizualAge: a novel approach to laser ablation ICP-MS U-Pb geochronology data reduction. *Geostand. Geoanal. Res*. 36, 247–270.

Poller U. 1997: U-Pb single zircon study of gabbroic and granitic rocks of Val Barlas-ch (Silvretta nappe, Switzerland). *Schweiz. Mineral. Petrogr. Mitt.* 77, 351–359.

Richter M. 1958: Über den Bau der nördlichen Kalkalpen im Rätikon. *Zeitschr. Deutsch. Geol. Ges.* 110, 307–325.

Ring U., Ratschbacher L., Frisch W., Biehler D. & Kralik M. 1989: Kinematics of the Alpine plate margin: structural styles, strain and motion along the Penninic-Austroalpine boundary in the Swiss-Austrian Alps. *J. Geol. Soc., London* 146, 835–849.

Schaltegger U., Nägler T.F., Corfu F., Maggetti M., Galetti G. & Stosch H.G. 1997: A Cambrian island arc in the Silvretta nappe: constraints from geochemistry and geochronology. *Schweiz. Mineral. Petrogr. Mitt.* 77, 337–350.

Schulz B. 2008: Basement of the Alps. In: McCann T. (Ed.): Geology of Central Europe. Precambrian and Paleozoic, vol 1. *Geol. Soc.,* London, 79–83.

Schulz B., Bombach K., Pawlig S. & Brätz H. 2004: Neoproterozoic to Early-Palaeozoic magmatic evolution in the Gondwana-derived Austroalpine basement to the south of the Tauern Window (Eastern Alps). *Int. J. Earth Sci.* 93, 824–843.

Sláma J., Košler J., Condon D.J., Crowley J.L., Gerdes A., Hanchar J.M., Horstwood M.S.A., Morris G.A., Nasdala L., Norberg N., Schaltegger U., Schoene N., Tubrett M.N. & Whitehouse M.J. 2008: Plešovice zircon — A new natural reference material for U-Pb and Hf isotopic microanalysis. *Chem. Geol.* 249, 1–35.

Spillmann P. & Büchi H.J. 1993: The Pre-Alpine Basement of the Lower Austro-Alpine Nappes in the Bernina Massif (Grisons, Switzerland; Valtellina, Italy). In: von Raumer J.F. & Neubauer F. (Eds.): Pre-Mesozoic Geology in the Alps. *Springer*, 457–467.

Stahel A.H. 1926: Geologische Untersuchungen im nordöstlichen Rätikon. *Dissertation, Universität Zürich*, 1–82.

Streckeisen A. 1948: Der Gabbrozug Klosters-Davos-Arosa. *Schweiz. Mineral. Petrogr. Mitt.* 28, 195–214.

Tollmann A. 1970: Der Deckenbau der westlichen Nordkalkalpen. *Neu. Jb. Geol. Paläont. Abh.* 136, 80–133.

von Quadt A. 1992: U-Pb zircon and Sm-Nd geochronology of mafic and ultramafic rocks from the central part of the Tauern Window (eastern Alps). *Contrib. Mineral. Petrol.* 110, 57–67.

von Quadt A., Grünenfelder M. & Büchi H.J. 1994: U-Pb zircon ages from igneous rocks of the Bernina nappe system (Grison, Switzerland). *Schweiz. Mineral. Petrogr. Mitt*. 74, 373–382.

von Raumer J.F., Stampfli G.M. & Bussy F. 2003: Gondwana-derived microcontinents: The constituents of the Variscan and Alpine collisional orogens. *Tectonophysics* 365, 7–22.

von Raumer J.F., Bussy F., Schaltegger U., Schulz B. & Stampfli G.M. 2013: Pre-Mesozoic Alpine basements — their place in the European Paleozoic framework. *Geol. Soc. Amer. Bull.* 125, 89–108.

von Seidlitz W.1906: Geologische Untersuchungen im östlichen Rätikon. *Ber. Naturf. Ges. Freiburg i.B.* 16, 232–366.

Wiedenbeck M., Alle P., Corfu F., Griffin W.L., Meier M., Oberli F., von Quadt A., Roddick J.C. & Spiegel W. 1995: Three natural zircon standards for U-Th-Pb, Lu-Hf, trace element and REE analyses. *Geostand. Newslett.* 19, 1–23.

Wiedenbeck M., Hanchar J.M., Peck W.H., Sylvester P., Valley J., Whitehouse M., Kronz A., Morishita Y. & Nasdala L. 2004: Further characterisation of the 91500 zircon crystal. *Geostand. Geoanal. Res.* 28, 9–39.

Wilson M. 1989: Igneous Petrogenesis. *Unwin Hyman*, London, 1–466.

Table S1: LA-ICP-MS U-Th-Pb zircon dating methodology, Steinmann-Institut, Bonn, Germany.

Laboratory & Sample Preparation	
Laboratory name	Steinmann-Institut, Rheinische Friedrich Wilhelms-Universität Bonn
Sample type/mineral	Meta-Diorite/ igneous and inherited zircons
Sample preparation	conventional mineral separation (SPT), 1 inch resin mount, 1 µm polish
Imaging / characterization	CL, Jeol 8200 Superprobe
Acquisition date & sequence name	2014-01-30_Zircon2.seq
Laser Ablation System	
Make, model & type	Resonetics Resolution M-50E 193nm excimer
Ablation cell & volume	Laurin Technic two-volume cell, effective volume 1-2 cm^3
Laser wavelength	193 nm
Pulse width	5 ns
Fluence	~ 9 J/cm^2 (5mJ, 100%T)
Repetition rate	10 Hz
Spot size	33 µm
Sampling mode / pattern	single spot analyses
Carrier gas	100% He, 650 ml/min He
Background collection	27 s
Ablation duration	30 s
Wash-out delay	8 s (post-ablation) + 60 s (after 3 cleaning pulses, 58 µm)
ICP-MS Instrument	
Make, model & type	Thermo Scientific Element XR single collector SF-ICP-MS
Sample introduction	via conventional tubing, no squid
RF power	1250 W
Ar gas flows	cooling: 16 l/min, auxiliary: 0.80 l/min, sample: 1.28 l/min,
Detection system	single collector secondary electron multiplier (counting mode)
Masses measured	202, 204, 206, 207, 208, 232, 238
Integration time per peak	4 x 40 ms (202, 204, 207), 4 x 10 ms (206, 208, 232), 10 x 4 ms (238)
Integration time per reading	650 ms (65 s / 100 runs)
Sensitvity	7430 cps/ppm U (238 on NIST SRM 612 at measurement conditions)
Dead time	2 ns (dead time correction applied)
Data Processing	
Calibration strategy	91500 used as primary reference material, Plešovice used as secondary reference materials.
Reference material info	91500 (1065.4 ± 0.6 Ma, Wiedenbeck et al. 1995, 2004) Plešovice (337.1 ± 0.4 Ma, Sláma et al. 2008)
Data processing package used / correction for LIEF	Iolite (Paton et al. 2011) with DRS VizualAge 2013.02 (Petrus & Kamber 2012). Isoplot (Version 3.75) (Ludwig 2012) was used for plotting and calculation of weighted mean ages.
Mass discrimination	Standard-sample bracketing with ratios normalized to primary reference zircon 91500.
Common-Pb correction, composition and uncertainty	Amount of common-Pb was insignificant (f206 < 0.5%), no correction applied.
Uncertainty level & propagation	Ages are quoted at 2 sigma absolute, within-run reproducibility and age uncertainty of reference material are propagated. A systematic error of 1.5 % is propagated by quadratic addition into the final population age.
Quality control / validation	Plešovice: 339.6 ± 1.7 Ma (2σ, MSWD of concordance = 0.24 and probability of concordance 0.63).

Table S2: LA-ICP-MS U-Pb isotopic data for Plešovice zircon reference material.

Analysis	Analysis	U	Th	Pb	^{206}Pb	^{238}U		Measured Isotopic Ratios							Ages [Ma]			
#	Name	[ppm]	[ppm]	[ppm]	[cps]	[cps]	f206%[a]	^{207}Pb/^{235}U	2σ	^{206}Pb/^{238}U	2σ	rho	^{207}Pb/^{206}Pb	2σ	^{207}Pb/^{235}U	2σ	^{206}Pb/^{238}U	2σ
11	Plesov_1	706	77	12	289611	4576425	0,08	0,4032	0,0087	0,05393	0,00086	0,28	0,05390	0,00095	343,8	6,3	338,6	5,3
21	Plesov_2	730	79	13	305525	4846501	0,00	0,3973	0,0088	0,05388	0,00082	0,30	0,05323	0,00094	339,5	6,3	338,3	5,0
31	Plesov_3	818	84	13	352652	5639379	-0,02	0,3928	0,0081	0,05356	0,00074	0,30	0,05299	0,00080	336,3	5,9	336,3	4,6
41	Plesov_4	737	80	13	321238	5108126	0,04	0,3994	0,0077	0,05394	0,00082	0,26	0,05352	0,00079	341,1	5,6	338,7	5,0
51	Plesov_5	818	98	15	360948	5706533	-0,01	0,4027	0,0087	0,05466	0,00078	0,09	0,05322	0,00093	343,4	6,3	343,0	4,7
61	Plesov_6	841	87	14	368157	5920307	-0,03	0,3949	0,0085	0,05384	0,00088	0,38	0,05299	0,00090	337,8	6,2	338,0	5,4
71	Plesov_7	774	83	13	339123	5392473	-0,15	0,3935	0,0083	0,05441	0,00093	0,45	0,05212	0,00086	336,8	6,0	341,5	5,7
77	Plesov_8	854	99	16	367928	5869538	0,05	0,4026	0,0076	0,05414	0,00081	0,22	0,05366	0,00078	343,4	5,5	339,9	5,0

[a]f206% denotes the fraction of ^{206}Pb that is common ^{206}Pb and is calculated with f206% = (^{207}Pb/^{206}Pb$_{measured}$ - ^{207}Pb*/^{206}Pb*) / (^{207}Pb/^{206}Pb$_{common}$ - ^{207}Pb*/^{206}Pb*)*100.

Table S3: LA-ICP-MS U-Pb isotopic data for 91500 zircon reference material.

Analysis	Analysis	U	Th	Pb	^{206}Pb	^{238}U		Measured Isotopic Ratios							Ages [Ma]			
#	Name	[ppm]	[ppm]	[ppm]	[cps]	[cps]	f206%[a]	^{207}Pb/^{235}U	2σ	^{206}Pb/^{238}U	2σ	rho	^{207}Pb/^{206}Pb	2σ	^{207}Pb/^{235}U	2σ	^{206}Pb/^{238}U	2σ
1	91500_1	81	30	15	113851	532304	-0,15	1,887	0,052	0,1835	0,0028	0,19	0,0744	0,0023	1075	18	1086	15
2	91500_2	81	30	15	110964	531960	-0,17	1,839	0,049	0,1793	0,0028	0,46	0,0734	0,0021	1058	17	1063	16
12	91500_3	79	31	15	106394	512589	-0,03	1,837	0,048	0,1791	0,0028	0,33	0,0745	0,0022	1058	17	1062	15
13	91500_4	76	29	15	102194	492913	0,26	1,896	0,050	0,1784	0,0031	0,51	0,0768	0,0020	1078	18	1058	17
22	91500_5	77	29	14	105570	514728	-0,02	1,814	0,044	0,1771	0,0029	0,26	0,0742	0,0020	1049	16	1051	16
23	91500_6	87	32	16	117969	578614	0,15	1,848	0,041	0,1764	0,0027	0,15	0,0755	0,0018	1062	15	1047	15
32	91500_7	83	30	15	118569	574915	-0,02	1,846	0,045	0,1787	0,0027	0,05	0,0745	0,0019	1061	16	1060	15
33	91500_8	82	30	15	115577	563905	0,21	1,858	0,048	0,1776	0,0028	0,44	0,0762	0,0021	1065	17	1054	16
42	91500_9	81	31	16	114453	557910	-0,05	1,820	0,047	0,1781	0,0031	0,19	0,0741	0,0021	1051	17	1056	17
43	91500_10	76	29	15	108282	525510	-0,01	1,835	0,054	0,1791	0,0033	0,39	0,0747	0,0023	1060	21	1062	18
52	91500_11	79	29	15	112688	550066	0,09	1,867	0,049	0,1795	0,0031	0,45	0,0756	0,0020	1068	18	1064	17
53	91500_12	81	32	15	116645	562994	-0,06	1,854	0,041	0,1803	0,0028	0,24	0,0745	0,0019	1067	14	1069	15
62	91500_13	82	31	15	118953	575344	-0,03	1,857	0,046	0,1801	0,0028	0,33	0,0747	0,0020	1065	16	1067	15
63	91500_14	81	30	15	117556	568638	0,00	1,856	0,048	0,1793	0,0031	0,19	0,0748	0,0022	1064	17	1063	17
72	91500_15	79	29	15	111564	550225	0,06	1,825	0,044	0,1767	0,0032	0,39	0,0748	0,0019	1053	16	1049	17
73	91500_16	83	31	16	117969	572438	0,00	1,861	0,055	0,1798	0,0030	0,22	0,0749	0,0023	1065	20	1066	16
78	91500_17	79	30	15	111448	537763	-0,02	1,869	0,044	0,1806	0,0027	0,05	0,0749	0,0020	1069	16	1070	15

[a]f206% denotes the fraction of ^{206}Pb that is common ^{206}Pb and is calculated with f206% = (^{207}Pb/^{206}Pb$_{measured}$ - ^{207}Pb*/^{206}Pb*) / (^{207}Pb/^{206}Pb$_{common}$ - ^{207}Pb*/^{206}Pb*)*100.

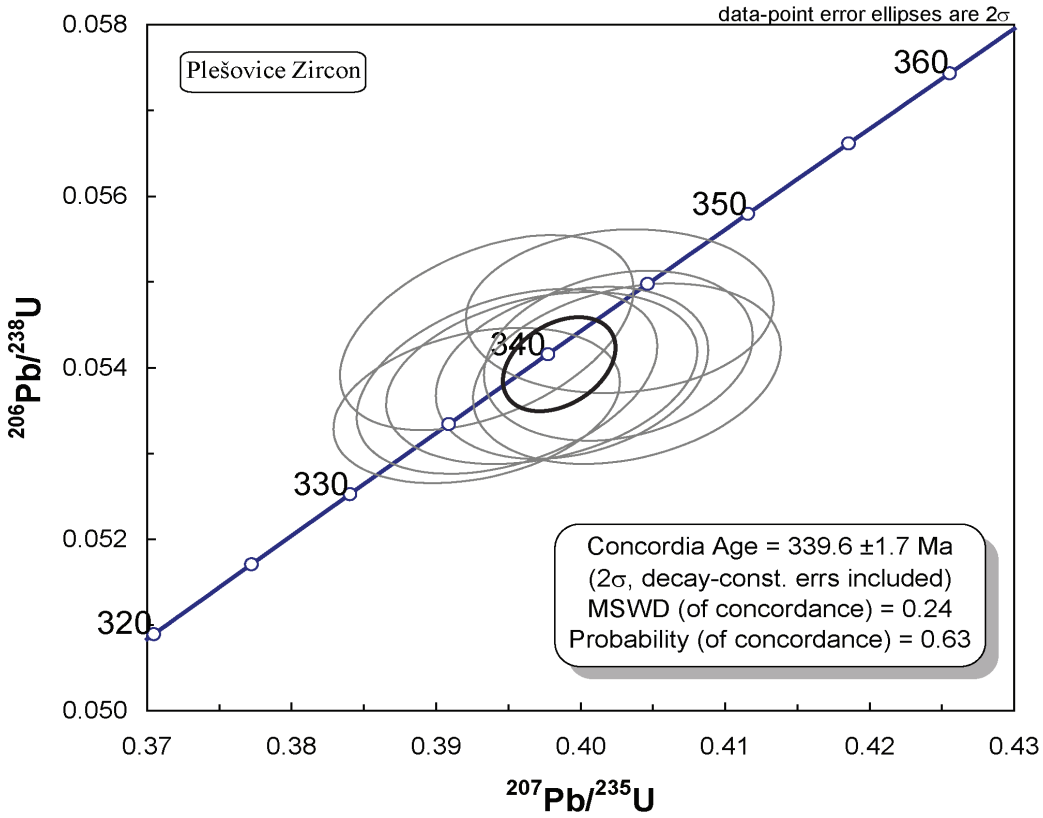

Fig. S4. Resulting concordia diagram for the measured Plešovice zircon reference material.